# Nanostructured Crystalline Comb Polymer of Perylenebisimide by Directed Self-Assembly: Poly(4-vinylpyridine)-pentadecylphenol Perylenebisimide

*Rekha Narayan, Prashant Kumar, K. S. Narayan, and S. K. Asha**

**Well defined nanostructured polymeric supramolecular assemblies are formed when an asymmetric perylenebisimide substituted with ethylhexyl chains on one end and functionalized with 3-pentadecylphenol at the other termini (PDP-UPBI) is complexed with poly(4-vinylpyridine) (P4VP) via a non-covalent specific interaction such as hydrogen-bonding. The resulting P4VP(PDP-UPBI)$_n$ complexes are fully solution processable. The bulk structure and morphologies of the supramolecular film studied using small angle and wide angle X-ray scattering reveals highly crystalline nature of the complex. Thin film morphology of the 1:1 complex analyzed using transmission electron microscopy shows uniform lamellar structures in the domain range of 5–10 nm. A clear trend of improved electrical parameters in P4VP(PDP-UPBI) system compared to pristine (PDP-UPBI) is observed from space charge limited current measurements. In short, a simple and facile method to obtain spatially defined organization of n-type semiconductor perylenebisimide molecules using hydrogen bonding interactions with P4VP as the structural motif is showcased herein.**

## 1. Introduction

Solution processable nanostructured functional materials (small molecules and polymers) with tailored property profiles have emerged as an indispensable requirement for organic photovoltaic technology as they constitute the building blocks essential for the design of organic and large area electronics (OLAE). These organic semiconductor materials form the integral part of several thin film based optoelectronics applications such as organic field effect transistors (OFETS), light emitting diodes (LED), solar cells, nanometer-scale lasers, optical waveguides, as well as super high density memory devices.[1–6] Whether it is a small molecule or a polymer based organic semiconductor, intermolecular interactions are of chief importance in controlling charge carrier mobility and higher mobilities can be achieved when the electronic coupling between the adjacent molecules is maximized. Therefore, it is highly desirable to assemble the semiconductor molecules at the nanometer scale. Thin film morphology is yet another equally important parameter that is in demand for uninterrupted charge transport pathways. Ideally a defect-free morphology can be provided by extremely pure organic single crystals grown from small molecules giving rise to a perfect charge transport system.[6,7] If it were possible to combine the ready processability of polymers with defect-free crystalline morphology of small molecules, a breakthrough can be expected in this area of research. The ultimate goal in the research on soft nanomaterials is to develop inexpensive, easy to fabricate solution processable crystalline materials with high charge carrier capacity.

In this regard, the research pioneered by the groups of Ikkala and ten Brinke on supramolecular comb coil diblock copolymers based on PS-b-P4VP (Polystyrene-block- poly(4 vinyl pyridine)) and surfactants like pentadecyl phenol (PDP) is very inspiring.[8–13] They showed that the hydrogen bonding interaction between the pyridine group of P4VP and hydroxyl group of PDP unit resulted in polymeric materials characterized by two length scales: the "block copolymer length scale" (10–100 nm) and a much shorter nanometer-scale (≈3 nm) due to the surfactant. Nanostructures could be formed with the homopolymer poly(4 vinyl pyridine) and PDP also, with different phase transitions observed depending on the balance of repulsive and attractive interactions.[14,15] The strong attractive hydrogen bonding interaction of the phenol with the nitrogen of pyridine is balanced by the repulsion between the alkyl side chains and the polar backbone. This concept of attaching small molecules to block copolymer based supramolecules was applied by the group of Rancatore et al. to an organic semiconductor like oligothiophene and P4VP resulting in solution processable nanostructured semiconductor composites with charge carrier mobilities comparable to the existing semiconductors already used in OPV devices.[16] Sun et al. developed a series of rod-coil diblock copolymers poly[2,7-(9,9-dihexylfluorene)]-*b*-poly(4-vinylpyridine) (PF-b-P4VP) and the P4VP coil blocks were hydrogen bonded with PDP which enabled different

R. Narayan, Dr. S. K. Asha
Polymer & Advanced Material Laboratory
Polymer Science & Engineering Division
CSIR, NCL,Pune-411008, Maharashtra, India
Fax: 0091-20-25902615
E-mail: sk.asha@ncl.res.in
P. Kumar, Prof. K. S. Narayan
Jawaharlal Nehru Centre for Advanced Scientific Research (JNCASR)
Jakkur, Bangalore, Karnataka, India

**DOI: 10.1002/adfm.201202366**

morphology transitions from lamellar to cylindrical or from cylindrical to spherical due to the increase of volume fraction of P4VP(PDP) comb blocks.[17] Stamm et al. further established that block copolymer and small molecule supramolecular assembly ensured patterning of functional materials into periodic structures in the nanoscopic length scale.[18,19]

Motivated by the plethora of successful accomplishments in the field of supramolecular assemblies (SMA), we have initiated a different step incorporating an n-type organic semiconductor molecule, perylenebisimide into polymer scaffold using secondary interactions. Among the arylenediimide based n-type (acceptor) semiconductors, perylene (PBI) and naphthalene (NBI) bisimides, PBI is most widely studied owing to the unique combination of high electron mobility, large molar absorption coefficients, excellent self-assembling ability, versatile structural modification as well as good thermal and photochemical stabilities.[20–24] However, their use in applications requires considerable effort to overcome their intrinsically low solubility and therefore the preparation of thin layers is carried out by the vapor deposition method. The alternative method of blending low molecular weight perylene imides with other polymers to prepare smooth films has the inherent problem of macrophase separation. In this context polymer based perylenebisimides had generated a lot of research interest. However, perylenebisimides when covalently tethered to a polymer backbone either in main chain or as side groups of block copolymers, gains in terms of solution processability and microphase separability, but looses out in terms of the intrinsic crystallinity of the small molecule.[25–27] Thus, the highest achieved electron mobility for low molecular weight PBIs[28–30] is 0.1–2 $cm^2\ V^{-1}\ s^{-1}$ whereas for solution processable PBI side chain homopolymers it is only of the order of $10^{-3}\ cm^2\ V^{-1}\ s^{-1}$.[31,32]

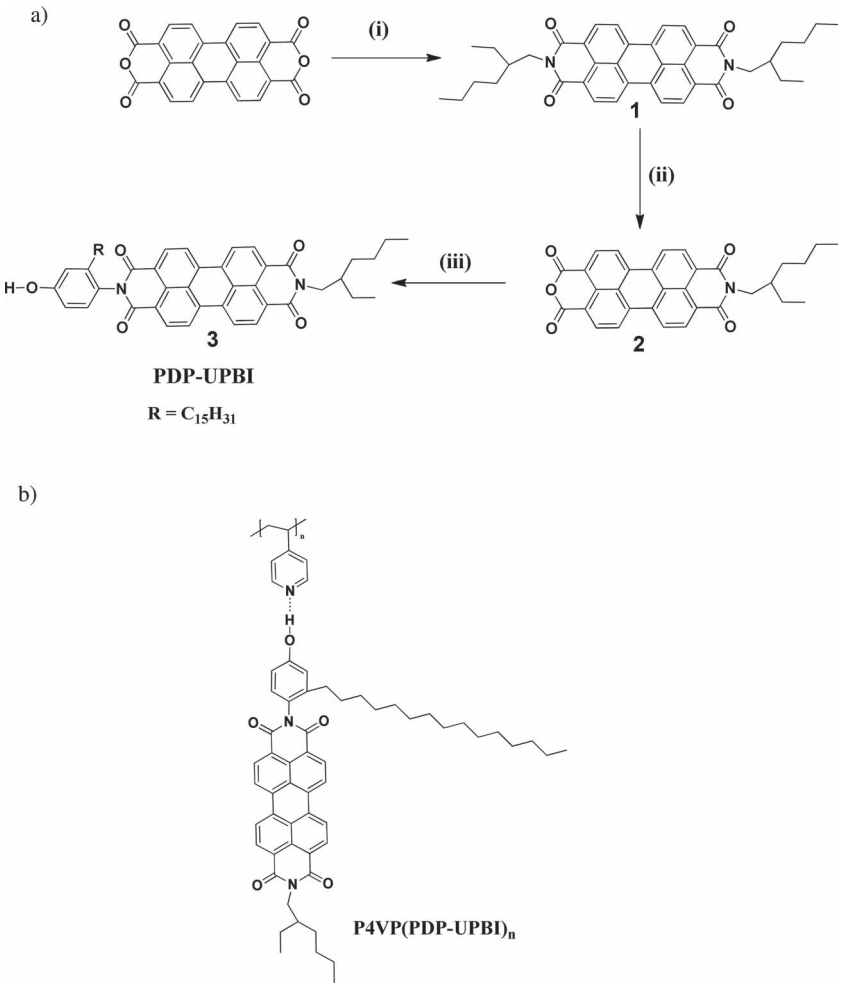


**Scheme 1.** a) Synthesis of asymmetrical **(PDP-UPBI)** Perylenebisimide. Reagents (i) 2-ethylhexylamine, N,N-dimethylacetamide(DMAc), $Zn(OAc)_2$, 110 °C, 4 h; (ii) KOH, *t*-BuOH, 90 °C 1-1.5 h; (iii) 4-amino-3-pentadecyl phenol, imidazole, $Zn(OAc)_2$, 2-4 h, 160 °C. b) Structure of complex formed by the asymmetrical **(PDP-UPBI)** with 4-vinylpyridine unit of P4VP polymer.

The present work describes our attempt at addressing the prevailing situation by combining solution processability with crystallinity in PBI derivatives by supramolecular complexation of a 3-pentadecylphenol based asymmetric perylenebisimide (**PDP-UPBI**) to poly(4-vinyl pyridine) (P4VP) polymer via hydrogen bonding. Various stoichiometric complexes of **P4VP(PDP-UPBI)**$_n$ where $n$ was varied from 0.25 to 1.00 were prepared and characterized. Complexation with P4VP was anticipated to induce solution processability as well as film forming property to the **PDP-UPBI** which were probed by the FTIR and $^1$H NMR studies. Bulk structure analyses by XRD experiments indicated that the polymeric complexes retained high crystallinity, which is very difficult to achieve in the case of polymer based systems. We also investigated the morphology of the polymer composites using TEM imaging which showed the presence of microphase separated nanostructures. The charge carrier mobility of these materials were studied using space charge limited current (SCLC) measurements. The study presented here provides a viable route towards low cost semiconducting materials with long range crystalline order favoring electronic coupling between molecular building blocks, processability as well as high electron mobility.

## 2. Results and Discussion

The supramolecular assembly of n-type organic semiconductor perylenebisimide (PBI) with poly(4-vinylpyridine) (**P4VP**), involving different non-covalent secondary interactions such as hydrogen-bonding, $\pi$–$\pi$ stacking and hydrophobic interactions were investigated. An asymmetric, perylenebisimide amphiphile (**PDP-UPBI)** having a 3-pentadecylphenol moiety which could involve in hydrogen bonding interaction with the pyridine units of P4VP, was synthesized and characterized for this study. The synthesis was carried out using reported literature procedure as shown in **Scheme 1**a.[33] The PBI derivative

was obtained in extremely pure form by repeated column chromatography purification procedures. The high level of purity was confirmed by the single peak in the SEC together with mass data and elemental analysis (see supporting information for details). The chemical structure of the **PDP-UPBI** complexed with poly(4-vinylpyridine) is depicted in Scheme 1b. The complex was prepared by dissolving different weight ratios of **PDP-UPBI** with fixed amounts of P4VP in DMF as solvent, stirring at ambient conditions for 24 h, followed by removal of solvent by heating. The complex was named **P4VP(PDP-UPBI)**$_n$, where $n$ denoted the theoretical ratio of **PDP-UPBI** to 4-vinylpyridine repeat units, which was varied from 0.25 to 1.00 in our study. The first hint of successful complexation was obtained from the increased solubility of the complex compared to the respective pure components. The formation of the complex was traced by FTIR spectroscopy as illustrated in literature for the complexes of P4VP with PDP.[14] P4VP has a symmetric ring stretching mode at 993 $cm^{-1}$ and a strong carbon-nitrogen stretching band at 1597 $cm^{-1}$ for free pyridine groups, which gets shifted to higher wavenumbers upon hydrogen bonding interaction with the phenol unit of PDP. The shift corresponding to the 1597 $cm^{-1}$ peak was difficult to trace in our PBI complex since pentadecylphenol unit attached to the perylene core also had absorption band in the same region. Another characteristic absorption band of pure P4VP around 1413 $cm^{-1}$ was devoid of any overlapping absorptions from pure **PDP-UPBI**. Ruokolainen et al. had shown that for the nominally fully complexed P4VP(PDP)$_{1.0}$, the 1413 $cm^{-1}$ band got shifted to 1421 $cm^{-1}$.[14] The FT-IR spectra comparing the 993 $cm^{-1}$ and 1413 $cm^{-1}$ region of the 1:1 complex (equal number of pyridine and phenol groups) **P4VP(PDP-UPBI)**$_{1.0}$ along with that of P4VP and **PDP-UPBI** showed (Supporting Information Figure S3.1) that the hydrogen bonding of the pyridine ring of P4VP with the phenol of **PDP-UPBI** was almost complete as indicated by the complete vanishing of 993 $cm^{-1}$ band, with the simultaneous appearance of two new bands at 1003 and 1023 $cm^{-1}$ corresponding to hydrogen bonded pyridine. Similarly, in the 1413 $cm^{-1}$ region, a new peak appeared at 1421 $cm^{-1}$ in **P4VP(PDP-UPBI)**$_{1.0}$ which also confirmed the complexation. In fact, the shift of the pristine pyridine bands at 993 $cm^{-1}$ and 1413 $cm^{-1}$ in the complex to higher wavenumbers was not an abrupt phenomenon. A gradual shift in the peak position was observed as the degree of complexation increased from $n = 0.25$ to 1.00. This can be clearly understood from the FT-IR plots of **P4VP(PDP-UPBI)**$_n$ complexes with $n = 0.25$, 0.50, 0.75, and 1.00 (Supporting Information Figure S3.2). When the degree of complexation was 0.25 the peak shift was relatively small and on going from 0.25 to 0.75, it increased further and achieved a maximum shift of +10 for 993 $cm^{-1}$ and +8 for 1413 $cm^{-1}$ in the 1:1 complexes. The band shift is usually small when the pyridine ring is hydrogen bonded to phenolic moieties. For protonation or coordination type of bonding, relatively larger +20 to +40 shifts have been reported.[34,35]

A detailed structural characterization of the complexes was carried out using proton NMR spectroscopy in deuterated chloroform or deuterated 1,1,2,2-tetrachloroethane. **Figure 1** compares the $^1$H NMR spectra of P4VP, and **PDP-UPBI** along with the 1:1 complex–**P4VP(PDP-UPBI)**$_{1.0}$ recorded in $CDCl_3$ at room temperature (25 °C). The **PDP-UPBI** molecule had sharp signals corresponding to the 8 aromatic protons in the region 8.74-8.56 ppm, and signals corresponding to the 3 aromatic protons of pentadecyl phenol (PDP) unit (labeled as c, e, and d) at 7.1 (d, 1H), 6.88 (s, 1H), and 6.72 (d, 1H) ppm, respectively. On the other hand, P4VP had two sets of broad signals corresponding to four aromatic pyridine protons with intensity distribution corresponding to two protons each at 8.32 (d, 2H, labeled "a") and 6.36 ppm (d, 2H, labeled "b") respectively. Detailed labeling of the other protons is also indicated in the figure. Upon comparison, it can be clearly seen that in the 1:1 complex all signals became broadened indicating an overall polymeric nature for the perylene protons also. The PBI core protons also showed an upfield chemical shift of 8.64–8.45 ppm. Signal broadening and upfield chemical shifts observed for the perylene core protons are due to the increase in $\pi$-stacking ring current shielding the neighboring protons.[36–41] Corresponding chemical shifts were observed for the P4VP protons also. The proton labeled "a" at 8.32 ppm underwent a downfield shift to 8.46 ppm (0.14 ppm difference) and merged with the broad perylene core protons with just a hump visible. This peak position could be confirmed from the proton integration value of 10 under the peaks in the range 8.64–8.46 ppm corresponding to 8 perylene + 2 pyridine protons which matched well in intensity with the two aliphatic protons labeled "f" at 4.16 ppm. The downfield shift of the two aromatic pyridine protons near to nitrogen occurs because the hydrogen bonding between the phenolic OH of **PDP-UPBI** and lone pair of electrons on nitrogen atom of pyridine decreases the electron density around the pyridine nitrogen atom, thereby deshielding the "a" protons of the pyridine ring. The "b" protons are affected less by this deshielding due to its increased distance away from the hydrogen bonding site and hence does not show any significant chemical shift from 6.38 to 6.44 ppm (0.06 ppm difference) upon complexation. The Supporting Information Figure S3.3 compares the expanded aromatic region (6–9 ppm) in the $^1$H NMR spectra of the **P4VP(PDP-UPBI)**$_n$ complexes for $n = 0.25$, 0.50, 0.75, and 1.0 with **PDP-UPBI**, which were recorded in deuterated tetrachloroethane (TCE). The relative ratio of the intensity of the 8 aromatic perylene ring protons (8.63 ppm) and the two aromatic pyridine protons ("a") of P4VP at 8.31 ppm, increased on going from $n = 0.25$ to $n = 1.0$ in the **P4VP(PDP-UPBI)**$_n$ complexes. At $n = 1.0$, both perylene and P4VP showed 1:1 ratio for their respective aromatic proton intensities giving strong support for the stochiometric 1:1 complex formation. Only in the 1:1 complex, i.e., **P4VP(PDP-UPBI)**$_{1.0}$, the integration value of 8 for eight PBI core protons corresponded to 2 each for the two sets of pyridine ring protons "a" and "b" of P4VP at 8.31 and 6.40 ppm respectively. The integration values for the other complexes with $n < 1$ suggested incomplete complexation with more uncomplexed nitrogen on P4VP.

The supramolecular organization in the complexes in the solid state was investigated using both wide angle and small angle X-ray analyses. SAXS recorded in the very low angular range, usually $\theta = 0.1$–$1.5°$ provides information regarding the morphology at the level of microphase separated structure of repeat distances upto 150 nm. On the other hand, WAXS is used to probe structure at the length scale of the crystal unit cell. Several mesomorphic structures like spheres, rods, cylinders, and lamellae are known for surfactant induced self-assembly in

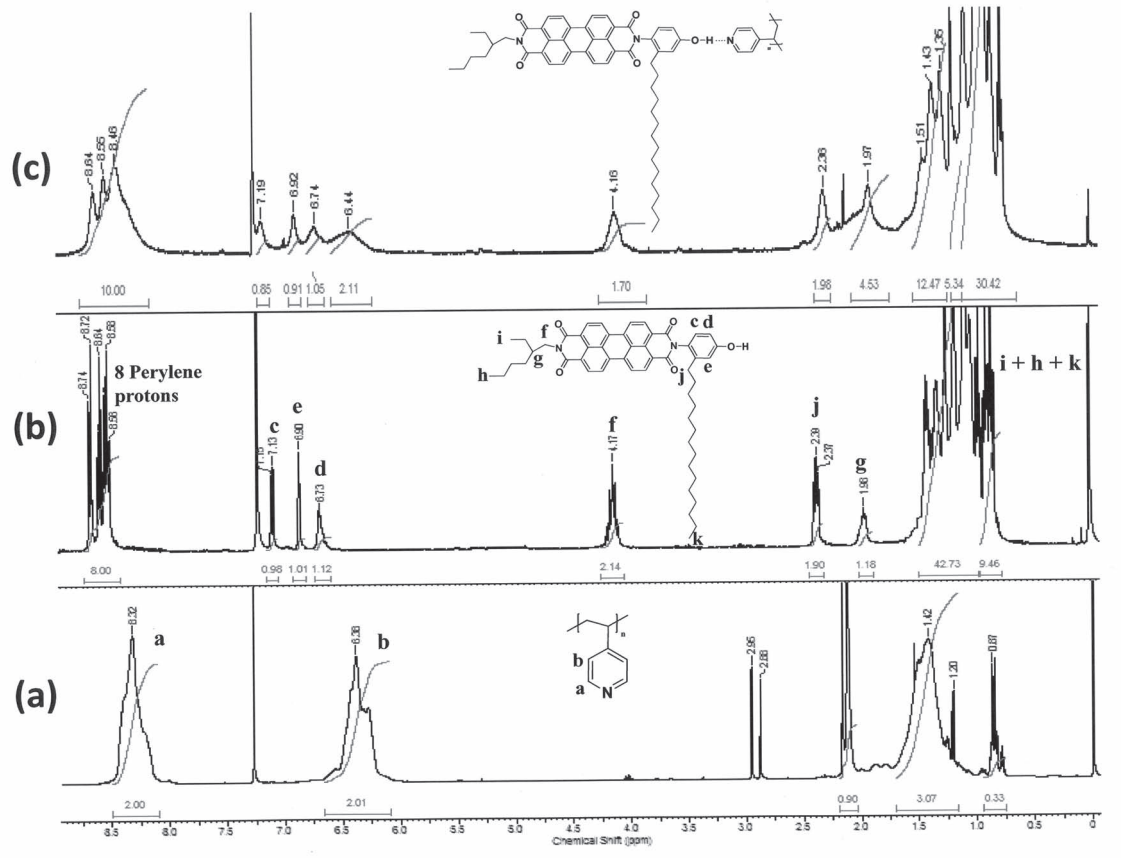


**Figure 1.** Comparison of $^1$H NMR spectra of a) **P4VP** b) **PDP-UPBI** and c) **P4VP(PDP-UPBI)**$_{1.0}$ recorded at 25 °C in $CDCl_3$ (15 mg/mL).

block copolymeric systems.[42–45] The hydrogen bonded systems formed by P4VP and PDP were shown to form lamellar structures.[46] Other morphologies like planar bilayers, perforated or undulating bilayers, cubic and hexagonal phases have also been reported for similar systems.[47–49] The perylene chromophore has a planar nature when the substituents are at the imide position. So it could be expected that the P4VP(PBI) complexes in the 1:1 case would ideally form planar bilayers or lamellae with alternating polymer layer and perylene layer, within which the perylenebisimide molecules would be self organized by $\pi$–$\pi$ stacking as well as the hydrophobic interactions such as interdigitation of the long C-15 alkyl chains. **Figure 2** shows the SAXS intensity curves obtained for **P4VP(PDP-UPBI)**$_n$ complexes at room temperature. The diffractograms of P4VP alone and **PDP-UPBI** are also included for comparison. Amorphous P4VP does not exhibit any peak in SAXS. The **PDP-UPBI** showed a distinct first order peak at $q^* = 0.196$ Å$^{-1}$ corresponding to a Bragg spacing ($d$) ≈32 Å, calculated using the formula $d = 2\pi/q$, where $q$ is the scattering vector. With increase in the degree of complexation from $n = 0.25$ to 1.0, the $q$ maxima also shifted to higher angle region (although the shift was small) leveling off to an interplanar spacing of $d \approx 31$ Å for the **P4VP(PDP-UPBI)**$_{1.0}$ complex. The inset in Figure 2 shows the complete 2D scattering pattern for the **P4VP(PDP-UPBI)**$_{1.0}$, from which the 1D data was obtained by azimuthal averaging. Unlike the

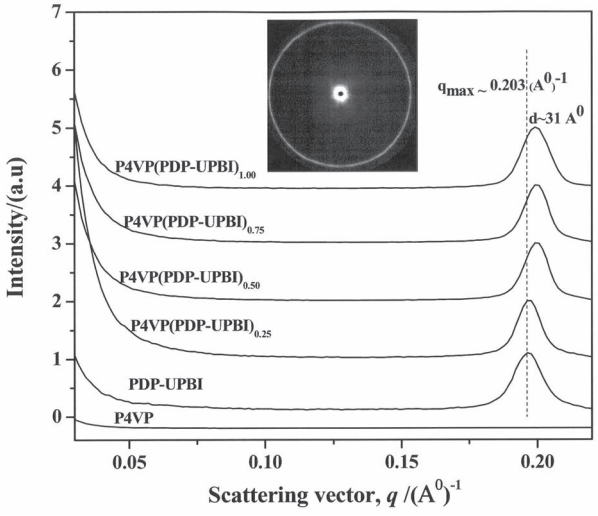


**Figure 2.** SAXS data for **P4VP(PDP-UPBI)**$_n$ complexes at room temperature. Inset shows the complete 2D pattern for **P4VP(PDP-UPBI)**$_{1.0}$.

SAXS data which had only very small shift (≈1 Å) in the primary reflection and no new structural features, the WAXS pattern showed dramatic changes. **Figure 3** shows the WAXS data for the same set of complexes measured at room temperature

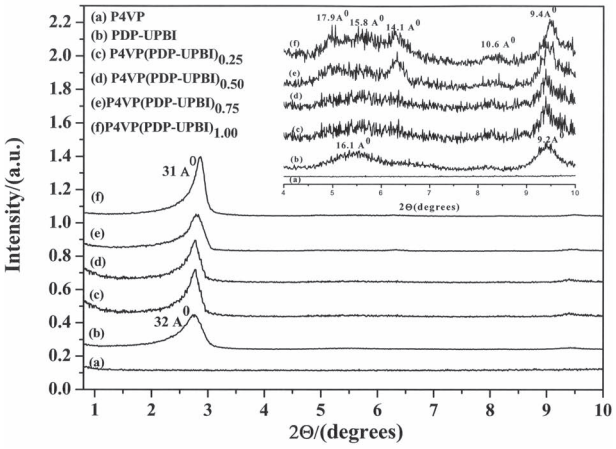


**Figure 3.** WAXS data ($2\theta = 0.5$–$10°$) for **P4VP(PDP-UPBI)**$_n$ complexes at room temperature. Inset shows the expanded region from $2\theta = 4$–$10°$.

(25 °C) in the range $2\theta = 0.5$–$10°$. The expanded $2\theta$ region from 4–10° is provided inset for clarification. Careful observation revealed the presence of faint higher order wave vectors indicating lamellar organization of this P4VP-PBI complex system for various compositions. **Table 1** shows the interlayer distances (Å) related to the reflections obtained from the WAXS pattern for the complexes as well as **PDP-UPBI**. It can be noted that **PDP-UPBI** itself showed distinct d-spacings estimated from Bragg reflections in the ratio 1: 1/2: 1/3, etc. typical of a layered structure, at 2.75° (32.04 Å), 5.49° (16.07 Å) and 8.21° (10.76 Å) respectively. In the **P4VP(PDP-UPBI)**$_n$ complexes, when the extent of complexation was small the interlayer separations were similar to that in **PDP-UPBI**, with the smallest interlayer separation observed for the 1:1 complex. At lower extents of complexation, for example when $n = 0.25$, the P4VP polymer is expected to form a thick layer between the PBI layers without causing much disturbance to it. As the extent of complexation was increased to 1:1 as in **P4VP(PDP-UPBI)**$_{1.0}$, the **PDP-UPBI** molecules are uniformly distributed along the P4VP backbone resulting in a thin polymer layer and maximum stretching and interpenetration of the alkyl chains of **PDP-UPBI** molecules. Additionally, some unexpected new structural changes were also observed in the $2\theta$ range 4.5–7° on moving from the pure **PDP-UPBI** to **P4VP(PDP-UPBI)**$_{1.0}$ complex. The second order reflection at 5.49° (16.07 Å) in **PDP-UPBI**, got transformed into 3 distinguishable peaks at 4.93° (17.91 Å), 5.57° (15.85 Å) and 6.27° (14.08 Å) upon complexation. This will be discussed later on when the WXRD studies measured from $2\theta$ range 2–35° will be analyzed. Generally, increased number of sharp reflections in the lower angle region is indicative of long range ordering at the nanometer scale.

Understanding the mode of assembly in **PDP-UPBI** would enable better insight into the bulk ordering of the complexes. Unfortunately, in spite of all attempts, we were unable to grow single crystals of the **PDP-UPBI** molecule. Therefore, we carried out energy minimization-DFT calculations using turbomole suit of programs for the **PDP-UPBI** molecule.[50,51] The resultant energy minimized structure of **PDP-UPBI** molecule viewed from different angles, with the different theoretically calculated length scales are shown in **Figure 4 (top)**. The perylene core adopted a planar geometry with the phenyl ring out of plane by 90°. The fully extended molecular length of **PDP-UPBI** from the phenolic oxygen at one end to the tip of the ethylhexyl substitution at the other end was 24.05 Å. Taking into account the non-planarity of the phenyl ring and the ethylhexyl chains, the distance from the phenolic oxygen through the perylene to the first $CH_2$ carbon of ethylhexyl substituent was 18.503 Å, i.e., the molecular axis along which the perylene core and phenyl ring lie in one line but perpendicular to each other (the ethylhexyl or pentadecyl $C_{15}$ chain does not lie in this line). From the energy minimized structure of PDP-UPBI it can be seen that the molecule had an approximate "V" shape with both the arms nearly equal in length. The WAXS showed a primary reflection at 31.86 Å corresponding to the interplanar spacing which could have originated by the interdigitation of the molecules either along the alkyl chain arm (21.6 Å × 2 = 42 Å) or the along the rigid perylene core (18.5 Å × 2 = 37 Å). The alkyl chains are known to undergo interdigitation in the all-trans conformation. In general, peaks for all trans extended chains are observed in the IR in the narrow range of 2846–2850 and 2915–2920 $cm^{-1}$, respectively, whereas bands in the range 2854–2856 and 2924–2928 $cm^{-1}$ indicate significant presence of gauche conformers.[52] In **PDP-UPBI** the alkyl chain bands were observed at 2924 and 2853 $cm^{-1}$ (Supporting Information

**Table 1.** Interlayer distances of the lamellar phase for **P4VP(PDP-UPBI)**$_n$ complexes and **PDP-UPBI** from the WAXS data recorded at room temperature (25 °C).

| Sample | Peak 1 | | Peak 2 | | | | | | Peak 3 | | Peak 4 | |
|---|---|---|---|---|---|---|---|---|---|---|---|---|
| | $2\theta$ [°] | d [Å] | Peak2(a) | | Peak2(b) | | Peak2(c) | | $2\theta$ [°] | $d$ [Å] | $2\theta$ [°] | $d$ [Å] |
| | | | $2\theta$ [°] | d [Å] | $2\theta$ [°] | d [Å] | $2\theta$ [°] | d [Å] | | | | |
| PDPUPBI | 2.75 | 32.04 | 5.49 | 16.07 | – | – | – | – | 8.21 | 10.76 | 9.43 | 9.37 |
| P4VP(PDPUPBI)$_{0.25}$ | 2.76 | 31.99 | 5.54 | 15.94 | – | – | – | – | 8.23 | 10.73 | 9.42 | 9.39 |
| P4VP(PDPUPBI)$_{0.50}$ | 2.78 | 31.82 | 5.47 | 16.10 | – | – | – | – | 8.27 | 10.68 | 9.39 | 9.41 |
| P4VP(PDPUPBI)$_{0.75}$ | 2.79 | 31.56 | 5.03 | 17.56 | 5.54 | 15.76 | 6.31 | 14.10 | 8.29 | 10.65 | 9.46 | 9.34 |
| P4VP(PDPUPBI)$_{1.00}$ | 2.86 | 30.93 | 4.93 | 17.91 | 5.57 | 15.85 | 6.27 | 14.08 | 8.31 | 10.64 | 9.50 | 9.31 |

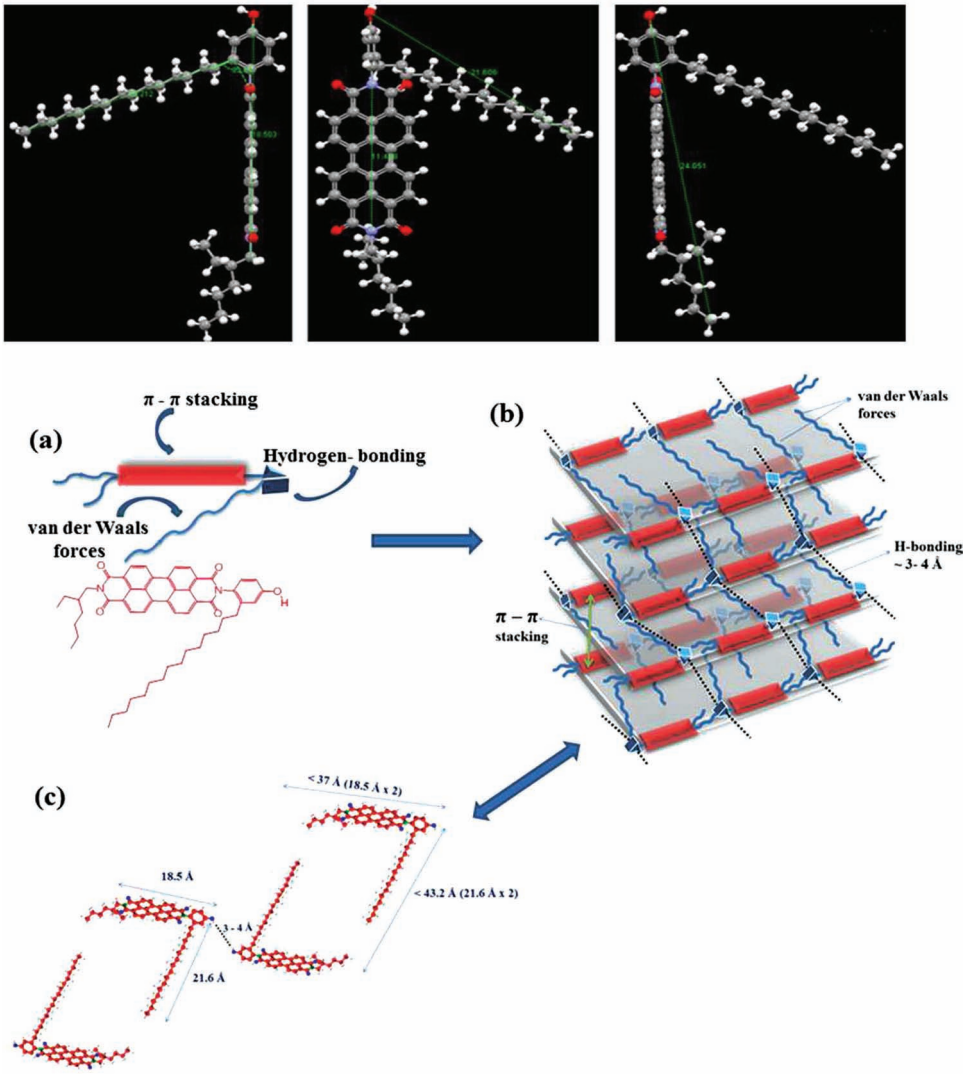


**Figure 4.** Top: Energy minimized DFT structures of **PDP-UPBI** viewed from a plane parallel and perpendicular to the perylene core. Bottom: a) schematic representation of **PDP-UPBI** molecule highlighting the various modes of self-assembly; b) schematic diagram showing 3D-mode of association of **PDP-UPBI** molecules; and c) 2D projection of alternate double layer involved in self-association.

Figure S3.4), which indicated considerable gauche conformers. These gauche conformers could be expected to hinder interdigitation of the long alkyl chains. Besides this, other observations based on WAXS data of the complex also suggested that packing along the rigid perylene core was more appropriate.

Based on these observations, a plausible mode of self-association among the **PDP-UPBI** molecules is given in Figure 4 (bottom). The different handles of self-assembly present within the single **PDP-UPBI** molecule, the hydrogen bonding with phenol head groups, $\pi$–$\pi$ stacking of conjugated perylene cores as well as the hydrophobic interaction between alkyl chains are also shown in Figure 4a. A co-operative interplay of these noncovalent interactions is expected to give rise to a three dimensional packing and crystallographic orientation as shown schematically in Figure 4b. The corresponding 2D view of two alternating planes using the DFT-energy minimized structures is also given in Figure 4c. The $\pi$–$\pi$ stacking of perylene cores between the adjacent layers occurs in conjunction with hydrogen bonding between phenolic –OH group on one **PDP-UPBI** molecule in one layer to that of another **PDP-UPBI** molecule lying diagonally opposite in the neighboring plane. In the solid state, molecules that can form hydrogen bonds tend to arrange themselves so as to maximize the formation of linear hydrogen bonds. Usually the distance of separation in a H-bond involving a proton donor (C–H, O–H, N–H) and a basic acceptor atom (O, N) is ≈3–4 Å, with strong directionality. But the strength of $\pi$–$\pi$ stacking is not as strong or as directional as the H-bonding. Therefore in the **PDP-UPBI** molecule H-bonding could be expected to stabilize the extended perylene core favoring longitudinal (interlayer) $\pi$–$\pi$ stacking as shown in Figure 4b) where the H-bond and $\pi$–$\pi$ stack direction were the same, within a 3–4 Å scale.

This packing model for the **PDP-UPBI** molecule was found to be in good correlation with the observed WXRD pattern. The **PDP-UPBI** molecule being highly crystalline, showed several sharp peaks in the entire $2\theta$ region in its room temperature powder WXRD pattern measured from $2\theta = 2–35°$ (Supporting Information Figure S3.5). The first and most intense sharp peak at 31.86 Å in the low angle region, which was noticeably larger than the individual molecule size, was assigned to the inter planar periodicity of **PDP-UPBI** layers, as explained earlier. The second peak observed at 16.11 Å closely matched the single molecule length of 18.5 Å between two ends of perylene core as demonstrated in Figure 4c. The peak at 10.76 Å corresponded to the length of perylene core alone obtained as 11.43 Å from DFT calculations. A comparatively broad reflection at $2\theta = 25.071°$ corresponding to a short range repeat distance of 3.56 Å could be attributed to $\pi$–$\pi$ stacking distance of adjacent perylene cores. Generally, only a diffused halo is observed in the $2\theta$ region beyond 15° when the alkyl chains have a liquid like conformation.[53] But in case of **PDP-UPBI** molecule several sharp peaks in the $2\theta = 15–22°$ range indicated highly ordered aliphatic components.

**Figure 5**a compares the WXRD of the complexes **P4VP(PDP-UPBI)**$_n$ with that of **PDP-UPBI** and P4VP in the range $2\theta = 3–35°$. It could be observed that the complexes remained highly crystalline with multiple sharp reflections in the entire $2\theta$ range from 3 to 27°, whereas pure P4VP showed only two broad halos - one around $2\theta = 11°$ and another at ≈20°.[54] The same observation of splitting of the peak at $2\theta = 5.47°$ upon complexation observed previously from the WAXS, was visible here also with more clarity. These three new spacings at 17.91 Å (4.93°), 15.85 Å (5.57°), and 14.08 Å (6.27°) in the **P4VP(PDP-UPBI)**$_{1.0}$ complex could be attributed to the internal structure of aromatic sublayers correlating with length scales derived from the energy minimized structure. The relative sharpness of all the reflections increased on going from **P4VP(PDP-UPBI)**$_{0.25}$ to **P4VP(PDP-UPBI)**$_{1.0}$ complexes. This could be considered as an indication of the increased ordering of the domains with increase in the extent of complexation. In the region $2\theta = 21–27°$, the peak at $2\theta \approx 25°$ corresponding to $\pi$–$\pi$ stacking distance (3.56 Å) was relatively broad in **PDP-UPBI** alone; a gradual increase was observed in this peak intensity with increase in the extent of complexation from $n = 0.25$ to 1.00. The 1:1 complex exhibited the highest intensity peak at $2\theta \approx 25.442°$ corresponding to $d = 3.50$ Å indicating an increase in the extent of $\pi$–$\pi$ stacking upon complexation. Additionally, a new peak around $2\theta \approx 26°$ (3.37Å) which was absent in **PDP-UPBI** was observed in the complex **P4VP(PDP-UPBI)**$_{0.25}$, and the intensity of this peak was highest in the **P4VP(PDP-UPBI)**$_{1.0}$ complex. This was further proof for well-defined ordering of domains even less than 3 Å, in the 1:1 P4VP-PBI complex, with the crystalline arrangement of complexes significantly differing from that of pure **PDP-UPBI**. In contrast, almost all of the reports on perylenebisimide polymers (main chain or side chain), in literature are conspicuous by the absence of peaks corresponding to crystallinity in the wide angle region.[55–57] In fact, the wide angle region in these polymers are characterized by featureless broad reflection where even the peak corresponding to d$\pi$–$\pi$ becomes visible only after significant magnification, indicating the loss of PBI crystallinity upon polymerization.[55–57] Retaining the high crystallinity of PBI derivative in a processable polymer format is the highlight of the approach reported here.

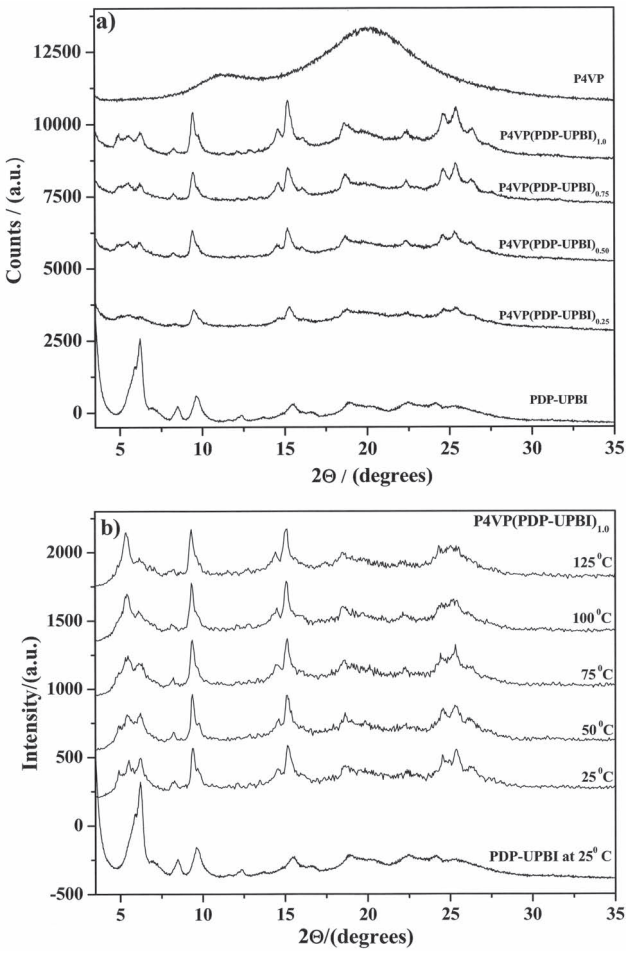


**Figure 5.** a) Wide angle X-ray diffraction pattern of **P4VP(PDP-UPBI)**$_n$ complexes from $2\theta = 3–35°$ recorded at 25 °C compared with that of **PDP-UPBI** and P4VP. b) Variable temperature Wide angle X-ray diffraction pattern of **P4VP(PDP-UPBI)**$_{1.0}$ complexes from $2\theta = 3–35°$.

The aggregation behavior of the complexes in the bulk state was further investigated by temperature dependent WXRD studies, since hydrogen bonding is known to break at higher temperatures. Figure 5b shows the variable temperature WXRD data for the **P4VP(PDP-UPBI)**$_{1.0}$ complex heated to 125 °C. The room temperature diffractogram of **PDP-UPBI** is also included for comparison. The three distinct spacings at 17.91 Å (4.93°), 15.85 Å (5.57°), and 14.08 Å (6.27°) in the **P4VP(PDP-UPBI)**$_{1.0}$ complex at room temperature showed significant changes upon increasing the temperature to 75 °C. Beyond 100 °C, the $\pi$–$\pi$ stacking region from $2\theta = 24–27°$ became featureless and the peaks around 15.85 and 14.08 Å almost vanished. The reflection at 17.91 Å which corresponded to the single molecule length also increased in intensity with increase in temperature. The changes in the peak pattern of the 1:1 complex with increase in temperature indicated a decrease in the degree of ordering which was originally present at room temperature. All these observations substantiated that complexation with P4VP

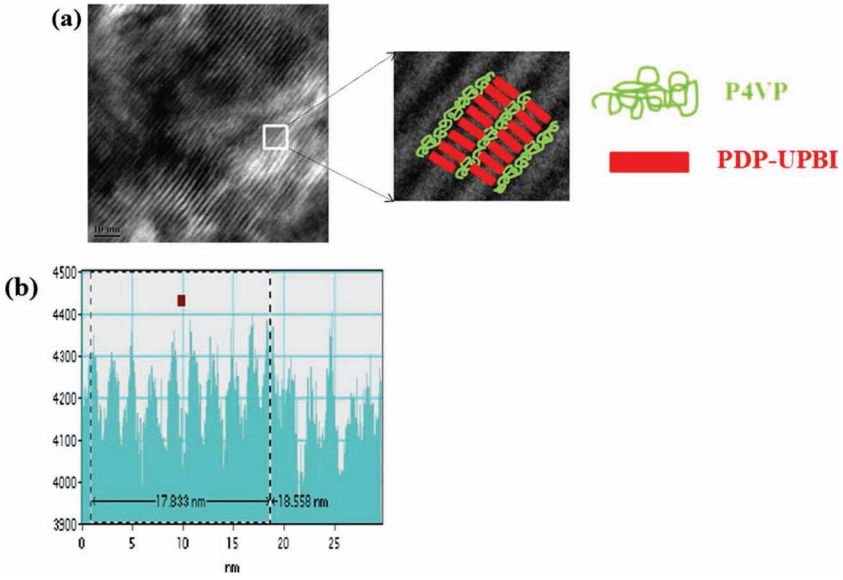


**Figure 6.** a) TEM image of thin film of **P4VP(PDP-UPBI)**$_{1.0}$ complex drop cast from 2 mg/mL DMF solution and stained with $I_2$ and b) histogram of the same image showing the individual layer thickness.

through hydrogen bonding had enhanced the nanometer-level organization within the crystalline **PDP-UPBI** domains with strengthened directionality.

Thin film morphology of the complex was analyzed using transmission electron microscopy (TEM). A representative TEM image of a very thin film of the **P4VP(PDP-UPBI)**$_{1.0}$ complex is shown in **Figure 6**. The histogram for the same nanostructure image automatically generated using Gatan Digital Micrograph software is also given. Attempts to get thin sections of the complex by microtoming failed since sections thinner than 110 nm could not be obtained. But we were fortunate enough to obtain good TEM images of the thin film morphology directly from drop cast samples. The thin film was drop cast from 2 mg/mL DMF solution onto the copper grid and stained with $I_2$ vapors to improve the contrast.[46] **PDP-UPBI** by itself did not show any specific pattern in TEM imaging under identical conditions (Supporting Information Figure S3.7). On the other hand, clear striated nanostructure formed by **P4VP(PDP-UPBI)**$_{1.0}$ lamellae could be clearly observed over a wide area (>100 nm) (Supporting Information Figure S3.6). The dark lines corresponded to the polar P4VP layers selectively stained by $I_2$, while the bright lines were the crystalline perylene blocks. The statistically averaged thickness of the bright line measured from the TEM image using the instrument software was ≈18.5 Å, which matched very well the perylene core length calculated from DFT. This lamellar structure could be described as a set of parallel planes formed by alternating P4VP and perylene layers. Since the self organization at the block copolymeric level occurs at 100–2000-Å length scale while that of simple homopolymer–amphiphile occurs at the 10–60-Å scale, the lamellar structure observed for **P4VP(PDP-UPBI)**$_{1.0}$ complex was appropriate at the 5–10-nm scale.

Based on the insight gathered from FT-IR, NMR, XRD, and morphological studies, evolution of the solution processable perylenebisimide nanostructured lamellae could be rationalized according to the cartoon given in **Figure 7**. The lengths shown are from the XRD data which were well correlated with that obtained from energy minimized structures. The **PDP-UPBI** molecule alone formed a loosely packed layered structure with a periodicity in between a completely non-interpenetrated end-to-end dimer (37 Å (18.5 Å × 2) and a monomer length (18.5 Å). Meanwhile in **P4VP(PDP-UPBI)**$_{1.0,}$ complexation resulted in a highly ordered lamellae with the **PDP-UPBI** monomers tightly packed with significant interpenetration leading to single layer structure. In **P4VP(PDP)**$_{1.0}$ the alkyl chains were shown to crystallize perpendicular to the plane formed by P4VP backbone.[58] But here in the **P4VP(PDP-UPBI)**$_{1.0}$ complex the steric demand by the rigid perylene core with phenol unit hydrogen bonding to the P4VP chain, confined the alkyl chain orientation in a plane almost parallel to that of P4VP backbone. The alternate parallel layers of P4VP and **PDP-UPBI** as viewed from the top is also shown.

The charge carrier mobility in the small molecule **PDP-UPBI** and **P4VP(PDP-UPBI)**$_{1.0}$ complex was evaluated using SCLC measurements. Clear space charge regime in $I(V)$ was observed in both the systems for most of the devices tested. The pristine **PDP-UPBI** as shown in **Figure 8**a exhibited the classical SCLC, $I = (9/8)\ \varepsilon\varepsilon_0\mu V^2/L^3$ regime, with a bulk mobility estimate of $\approx 10^{-6}$ cm$^2$ V$^{-1}$ s$^{-1}$. In case of the 1:1 complex, the trap modified behaviour in the $I(V)$ response was present, and a clear trend of higher conductance was observed for **P4VP(PDP-UPBI)**$_{1.0}$ compared to pristine **PDP-UPBI** devices as indicated by the magnitude of the current density for relatively thicker sample of the composite (Figure 8). The transport mechanism in **P4VP(PDP-UPBI)**$_{1.0}$ consisting of aggregate of ordered units is expected to be complex.The ordered segments distinctly enhances the transport parameters. The choice of a trap-free regime in $I(V)$ is apparently critical in the analysis. Both the Au and ITO coated devices yielded similar profiles. An analysis of a representative $I(V)$ obtained from studying several samples in the trap-free regime indicated mobility estimate of $\approx 10^{-3}$ cm$^2$ V$^{-1}$ s$^{-1}$ (Figure 8b) for **P4VP(PDP-UPBI)**$_{1.0}$.

## 3. Conclusions

In conclusion, we have shown that perylene bisimides, suitably functionalized for hydrogen bonding interactions, could be organized into lamellar structures in the domain range 5 to 10 nm using the concept of supramolecular assembly with poly(4-vinyl pyridine). A series of complexes of **P4VP(PDP-UPBI)**$_n$ with $n$ = 0.25, 0.50, 0.75, and 1.00 were prepared and characterized. Complexation improved the solubility and hence solution processability by several folds. Detailed structure and properties of the supramolecular assembly between **P4VP** and **PDP-UPBI** explored using FTIR, $^1$H NMR, SAXS, WAXS, and thin film morphology using TEM demonstrated the superior

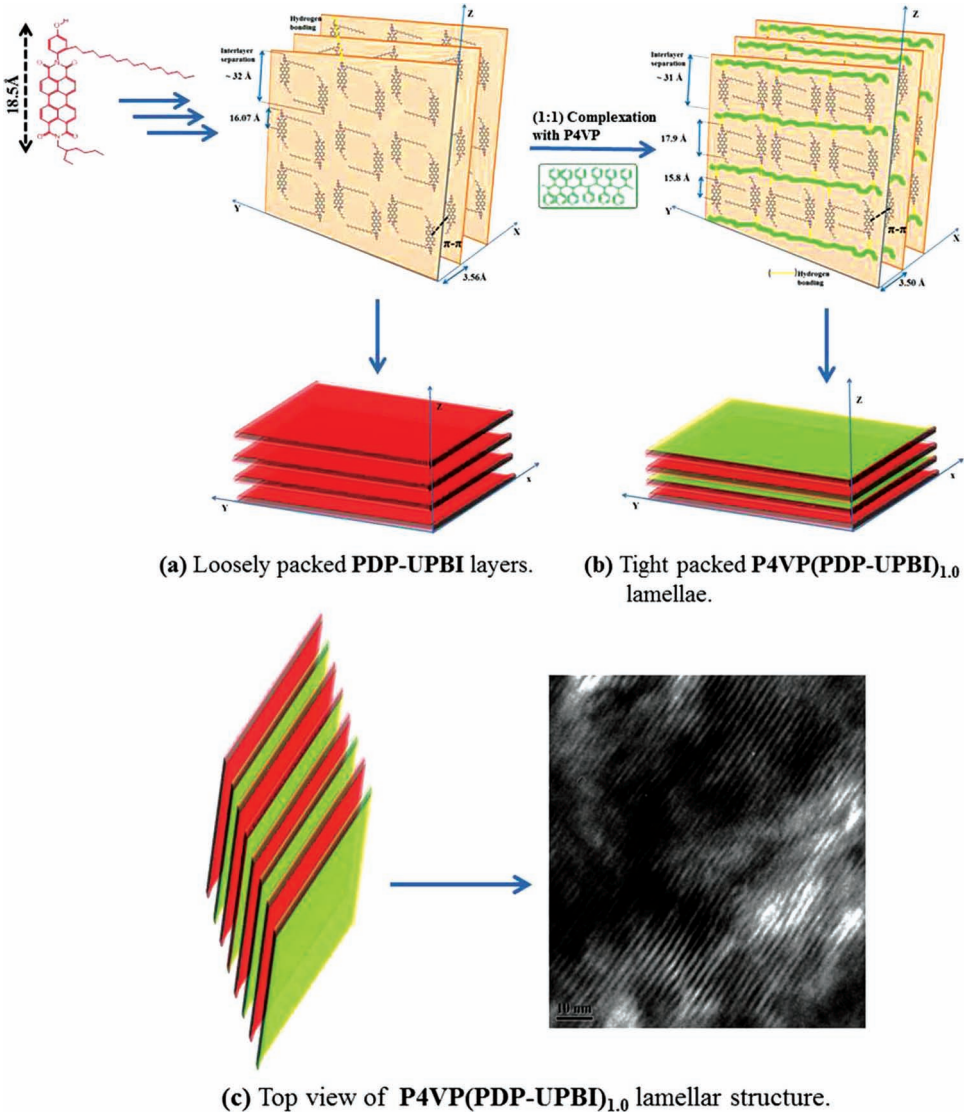


**Figure 7.** Proposed model for the nanostructure formation in **P4VP(PDP-UPBI)**$_{1.0}$ complex.

organization in the hydrogen bonded polymeric complex compared to the small molecule. The solid state studies using X-ray diffraction showed that both **PDP-UPBI** and its complexes with P4VP exhibited layered assembly. However, the packing order was drastically improved in the complex compared to the small molecule itself. Although both showed layered structure, only the complex could exhibit a phase separated nanostructure with ordering in the 5–10-nm range. Additional structural hierarchies can be obtained by introducing block copolymer based supramolecules like PS-b-P4VP. The most important highlight of this approach was the ability to retain the crystallinity of the perylene bisimide in the supramolecular polymer complex, thereby combining the advantage of the small molecule with the processability afforded by the polymer. SCLC mobility measurements of **P4VP(PDP-UPBI)**$_{1.0}$ indicated a clear trend of higher conductance compared to pristine **PDP-UPBI**. This concept is extendable to the analogous homologue with better charge transport properties–the naphthalene bisimides and also to the symmetric derivatives which can hydrogen bond through both terminals. Work along these lines is in progress.

## 4. Experimental Section

*Materials*: Poly(4-vinylpyridine) (P4VP) ($M_w$ = 60 000 Da) was purchased from Aldrich. It was dried in vacuum oven at 60 °C for 36 h prior to use. All solvents used were of analytical grade and carefully dried before use. All other chemicals used were purchased from Aldrich and used as received. Synthetic procedure to prepare the amphiphilic perylenebisimide (**PDP-UPBI**) is given in the Supporting Information.

*Sample Preparation*: Poly (4-vinylpyridine) (P4VP) as well as the amphiphilic perylenebisimide (**PDP-UPBI**) was dried in vacuum oven at 60 °C for 3 days. **P4VP(PDP-UPBI)**$_n$ complexes were prepared from dry

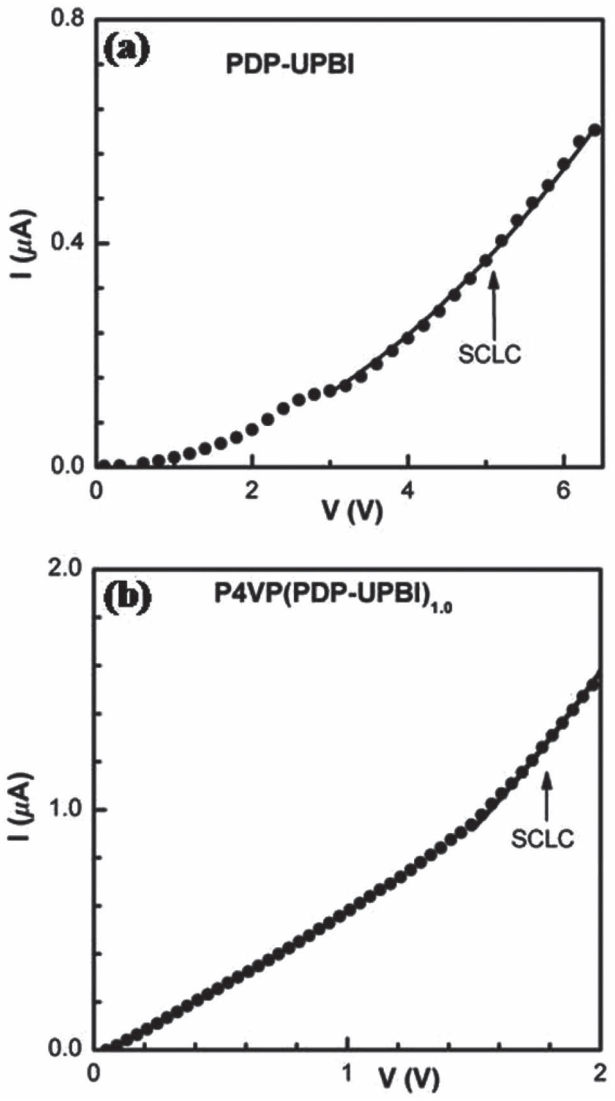


**Figure 8.** a) $I(V)$ of PDP-UPBI with ITO and Al electrodes (thickness ≈ 1.2 μm) and b) $I(V)$ of P4VP(PDP-UPBI)$_{1.0}$ with ITO and Al electrodes (thickness ≈ 7.3 μm). Dashed-line is a fit to the SCLC response.

DMF solutions, where *n* denotes the number of PBI molecules per vinyl pyridine (VP) repeat unit (n = **PDP-UPBI**/VP). In a typical procedure P4VP was first dissolved in DMF to which desired amount of **PDP-UPBI** was added depending on the value of *n* and the solution was stirred for 24 h. Concentration of the solutions were kept 1 wt%. Subsequently the solvent was evaporated slowly on a hot plate at 60 °C and further dried in vacuum oven at 65 °C for 3 days, slowly cooled to room temperature and stored in desiccator thereafter.

*Instrumentation Techniques*: Infrared spectra were obtained using Bruker α-T spectrophotometer in the range of 4000–400 cm$^{-1}$. **P4VP(PDP-UPBI)**$_n$ complexes dissolved in DMF were directly drop cast onto KBr pellets evaporated off slowly at 60–70 °C, followed by drying in vacuum oven overnight.$^1$H and $^{13}$C NMR spectra were recorded in $CDCl_3$using Bruker AVENS 200 MHz spectrophotometer. Chemical shifts ($\delta$) are reported in ppm at 298 K, with trace amount of tetramethylsilane (TMS) as internal standard. MALDI-TOF analysis was carried out on a Voyager-De-STRMALDI-TOF (Applied Biosystems, Framingham, MA, USA) instrument equipped with a 337 nm pulsed nitrogen laser used for desorption and ionization. The mode of operation was in a reflector mode with an accelerating voltage of 25 kV. Micromolar solutions of the compounds in THF were mixed with Dithranol matrix and spotted on stainless steel MALDI plate and dried well. The mode of operation was reflector mode with an acceleration voltage of 25 kV. Size exclusion chromatography (SEC) in THF was done using polystyrene standards for calibration. Waters 515 Pump connected through two series of Styragel HR columns (HR-3 and HR-4E) and Waters 2414 differential refractometer was used for analyzing the samples. The flow rate of the THF was maintained as 1 mL throughout the experiments, and 2–3 mg in 1mL of the samples were filtered and injected for recording the chromatograms at 30 °C. Thermogravimetric analysis (TGA) was performed using a PerkinElmer STA 6000 thermogravimetric analyzer. Samples were run from 40 to 800 °C with a heating rate of 10 °C/min under nitrogen. DSC (differential scanning colorimeter) measurements were performed on TA Q10 differential scanning calorimeter at a heating rate of 10 °C/min under nitrogen atmosphere. Typically, 3–4 mg of samples was placed in an aluminum pan, sealed properly and scanned from 10 °C/min. The instrument was calibrated with indium standards before measurements. The first heating cycles were avoided to get rid of thermal history of the samples. Wide angle X-ray diffractograms (WXRD) were obtained using a Philips analytical diffractometer with CuK$\alpha$ emission. All the samples were recorded in the ($2\theta$) range of 3–50° using a PANalyticalX'pert Pro dual goniometer diffractometer and analyzed using X'pert software. An X'celerator solid-state detector was employed in wide-angle experiments. The radiation used was CuK$\alpha$ (1.54 Å) with a Ni filter, and the data collection was carried out using a flat holder in Bragg–Brentano geometry. In situ XRD experiments were carried out using an Anton–Paar XRK900 reactor for high temperature measurements. Small angle X-ray scattering (SAXS) was employed to investigate the phase behaviour of the complexes. The scattering experiments were conducted on a three pinhole collimated Bruker Nanostar machine equipped with rotating copper anode, operating at 45 kV and 100 mA providing characteristic K$\alpha$ radiation of 1.54 Å. The measurements were carried out in the normal resolution mode having a q range of 0.011–0.2 Å$^{-1}$. The bulk sample was sandwiched between two Kapton films inside the sample holder. The scattered data was collected using a 2D Histar detector and later converted from 2D to 1D by azimuthal averaging using Bruker software. 1D data presented after background subtraction is plotted as $I$ vs $q$, where $q = (4\pi/\lambda)\ \mathrm{Sin}\theta$, $\lambda$ is the wavelength of the incident X-rays and $2\theta$ is the scattering angle. Transmission electron microscopy (TEM) was done using an FEI-Tecnai-F20 electron microscope operating at 200 kV. Sandwich structures on ITO coated glass and Au substrates were fabricated for the SCLC studies. Thin films of the samples were drop-cast and spin coated on the substrates. The thickness was determined using Dektak surface profiler. The top Al electrode defining the area of the film (0.1 cm$^2$) was coated using thermal deposition method in high vacuum. All measurements were carried out under inert atmosphere.

## Supporting Information

Supporting Information is available from the Wiley Online Library or from the author.

## Acknowledgements

This work has been financially supported by the network project NWP0054 and DST project SR/S1/OC-03/2009. The authors thank Mr. Pandiraj S. and Mr. Anuj Pokle, NCL–Pune for TEM imaging and Mr. Shrikant M K for the NMR measurement. R.N. thanks UGC-New Delhi, India for Senior Research Fellowship.

Received: August 18, 2012
Revised: October 16, 2012
Published online: November 22, 2012

[1] Q. Niu, Y. Zhou, L. Wang, J. Peng, J. Wang, J. Pei, Y. Cao, *Adv. Mater.* **2008**, *20*, 964.
[2] Q. Tang, L. Li, Y. Song, Y. Liu, H. Li, W. Xu, Y. Liu, W. Hu, D. Zhu, *Adv. Mater.* **2007**, *19*, 2624.
[3] H. Xin, F. S. Kim, S. A. Jenekhe, *J. Am. Chem. Soc.* **2008**, *130*, 5424.
[4] D. O'Carroll, I. Lieberwirth, G. Redmond, *Nat. Nanotechnol.* **2007**, *2*, 180.
[5] K. Takazawa, Y. Kitahama, Y. Kimura, G. Kido, *Nano Lett.* **2005**, *5*, 1293.
[6] K. Xiao, J. Tao, Z. Pan, A. A. Puretzky, I. N. Ivanov, S. J. Pennycook, D. B. Geohegan, *Angew. Chem. Int. Ed.* **2007**, *46*, 2650.
[7] J. H. Schön, Ch. Kloc, A. Dodabalapur, B. Batlogg, *Science* **2000**, *289*, 599.
[8] J. Ruokolainen, R. Mäkinen, M. Torkkeli, R. Serimaa, T. Mäkelä, G. ten Brinke, O. Ikkala, *Science* **1998**, *280*, 557.
[9] J. Ruokolainen, G. ten Brinke, O. Ikkala, *Adv. Mater.* **1999**, *11*, 777.
[10] K. de Moel, A. G. O. R. van Ekenstein, H. Nijland, E. Polushkin, G. ten Brinke, *Chem. Mater.* **2001**, *13*, 4580.
[11] O. Ikkala, G. ten Brinke, *Science* **2002**, *295*, 2407.
[12] O. Ikkala, G. ten Brinke, *Chem. Commun.* **2004**, *2*, 131.
[13] W. van Zoelen, T. Asumaa, J. Ruokolainen, O. Ikkala, G. ten Brinke, *Macromolecules* **2008**, *41*, 3199.
[14] J. Ruokolainen, G. ten Brinke, O. Ikkala, *Macromolecules* **1996**, *29*, 3409.
[15] J. Ruokolainen, M. Torkkeli, R. Serimaa, E. Komanschek, G. ten Brinke, O. Ikkala, *Macromolecules* **1997**, *30*, 2002.
[16] B. J. Rancatore, C. E. Mauldin, S.-H. Tung, C. Wang, A. Hexemer, J. Strzalka, J. M. J. Fréchet, T. Xu, *ACS Nano* **2010**, *4*, 2721.
[17] H.-S. Sun, C.-H. Lee, C.-S. Lai, H.-L. Chen, S.-H. Tung, W.-C. Chen, *Soft Matter* **2011**, *7*, 4198.
[18] B. Nandan, B. K. Kuila, M. Stamm, *Eur. Polym. J.* **2011**, *47*, 584.
[19] B. Nandan, M. K. Vyas, M. Böhme, M. Stamm, *Macromolecules* **2010**, *43*, 2463.
[20] F. Würthner, *Chem. Commun.* **2004**, *14*, 1564.
[21] G. Horowitz, F. Kouki, P. Spearman, D. Fichou, C. Nogues, X. Pan, F. Garnier, *Adv. Mater.* **1996**, *8*, 242.
[22] H. Langhals, *Helv. Chim. Acta.* **2005**, *88*, 1309.
[23] H. Langhals, *Heterocycles* **1995**, *40*, 477.
[24] Y. Avlasevich, C. Li, K. Müllen, *J. Mater. Chem.* **2010**, *20*, 3814.
[25] *Handbook of Organic Conductive Molecules and Polymers*, Vol. *4* (Ed: H. S. Nalwa), John Wiley & Sons, New York **1997**, Ch. 1.
[26] K. V. Rao, R. Haldar, C. Kulkarni, K. T. Maji, S. J. George, *Chem. Mater.* **2012**, *24*, 969.
[27] A. S. Lang, M. Thelakkat, *Polym. Chem.* **2011**, *2*, 2213.
[28] B. A. Jones, A. Facchetti, M. R. Wasielewski, T. J. Marks, *J. Am. Chem. Soc.* **2007**, *129*, 15259.
[29] R. J. Chesterfield, J. C. McKeen, C. R. Newman, P. C. Ewbank, D. A. D. Filho, J. Brédas, L. L. Miller, K. R. Mann, C. D. Frisble, *J. Phys. B* **2004**, *108,* 19281.
[30] S. Tatemichi, M. Ichikawa, T. Koyama, Y. Taniguchi, *Appl. Phys. Lett.* **2006**, *89*, 112108.
[31] S. Hüttner, M. Sommer, M. Thelakkat, *Appl. Phys. Lett.* **2008**, *92*, 093302.
[32] X. Zhan, Z. Tan, B. Domercq, Z. An, X. Zhang, S. Barlow, Y. Li, D. Zhu, B. Kippelen, S. R. Marder, *J. Am. Chem. Soc.* **2007**, *129*, 7246.
[33] A. Wicklein, A. Lang, M. Muth, M. Thelakkat, *J. Am. Chem. Soc.* **2009**, *131*, 14442.
[34] O. Ikkala, J. Ruokolainen, G. ten Brinke, M. Torkkeli, R. Serimaa, *Macromolecules* **1995**, *28*, 7088.
[35] J. Ruokolainen, O. Ikkala, J. Tanner, G. ten Brinke, M. Torkkeli, R. Serimaa, *Macromolecules* **1995**, *28*, 7779.
[36] J. Wang, A. Kulago, W. R. Browne, B. L. Feringa, *J. Am. Chem. Soc.* **2010**, *132*, 4191.
[37] W. Wang, L.-S. Li, G. Helms, H.-H. Zhou, A. D. Q. Li, *J. Am. Chem. Soc.* **2003**, *125*, 1120.
[38] J. S. Waugh, R. W. Fessenden, *J. Am. Chem. Soc.* **1957**, *79*, 846.
[39] D. J. Edwards, J. W. Jones, O. Lozman, A. P. Ormerod, M. Sintyureva, G. J. T. Tiddy, *J. Phys. Chem. B* **2008**, *112*, 14628.
[40] R. B. Martin, *Chem. Rev.* **1996**, *96*, 3043.
[41] J. C. Nelson, J. G. Saven, J. S. Moore, P. G. Wolynes, *Science* **1997**, *277*, 1793.
[42] W. van Zoelen, T. Asumaa, J. Ruokolainen, O. Ikkala, G. ten Brinke, *Macromolecules* **2008**, *41*, 3199.
[43] J. Wang, W. H. de Jeu, P. Müller, M. Möller, A. Mourran, *Macromolecules* **2012**, *45*, 974.
[44] W.-T. Chuang, H.-W. Shen, U.-S. Jeng, H.-H. Wu, P.-D. Hong, J.-J. Lee, *Chem. Mater.* **2009**, *21*, 975.
[45] S. Valkama, T. Ruotsalainen, A. Nykänen, A. Lahio, H. Kosonen, G. ten Brinke, O. Ikkala, J. Ruokolainen, *Macromolecules* **2006**, *39*, 9327.
[46] J. Ruokolainen, J. Tanner, O. Ikkala, *Macromolecules* **1998**, *31*, 3532.
[47] M. Antonietti, C. Burger, J. Eiffing, *Adv. Mater.* **1995**, *7*, 751.
[48] S. Zhou, F. Yeh, C. Burger, B. Chu, *J. Phys. Chem. B* **1999**, *103*, 2107.
[49] M. Antonietti, J. Conrad, *Angew. Chem. Int. Ed.* **1994**, *33*, 1869.
[50] R. Ahlrichs, M. Bär, H. P. Baron, R. Bauernschmitt, S. Böcker, M. Ehrig, K. Eichkorn, S. Elliott, F. Furche, F. Haase, M. Häser, H. Horn, C. Huber, U. Huniar, M. Kattannek, C. Kölmel, M. Kollwitz, K. May, C. Ochsenfeld, H. Öhm, A. Schäfer, U. Schneider, O. Treutler, M. von Arnim, F. Weigend, P. Weis, H. Weiss, *TURBOMOLE* (Version 5.3); Universität Karlsruhe, Karlruhe, Germany **2000**.
[51] A. D. Becke, *Phys. Rev. A* **1988**, *38*, 3098.
[52] S.-H. Park, C. E. Lee, *Chem. Mater.* **2006**, *18*, 981.
[53] Y. Huang, Y. Yan, B. M. Smarsly, Z. Wei, C. F. J. Faul, *J. Mater. Chem.* **2009**, *19*, 2356.
[54] S. Valkama, O. Lehtonen, K. Lappalainen, H. Kosonen, P. Castro, T. Repo, M. Torkkeli, R. Serimaa, G. ten Brinke, M. Leskelä, O. Ikkala, *Macromol. Rapid Commun.* **2003**, *24*, 556.
[55] Z. Zhou, J. L. Brusso, S. Holdcroft, *Chem. Mater.* **2010**, *22*, 2287.
[56] A. S. Lang, A. Neubig, M. Sommer, M. Thelakkat, *Macromolecules* **2010**, *43*, 7001.
[57] A. S. Lang, M. Thelakkat, *Polym. Chem.* **2011**, *2*, 2213.
[58] M. C. Luyten, G. O. R. A. van Ekenstein, G. ten Brinke, *Macromolecules* **1999**, *32*, 4404.